Supporting Information

Chiu et al. 10.1073/pnas.1418798112

SI Methods

Spindle Purification and Determination of the WEV Fusolin Sequence. Spindles were isolated from infected *Melolontha melolontha* collected from the field (1) and from reared *Anomala cuprea* (2) as described previously. *Wiseana* spp. larvae were field collected and screened for WEV infection. A fat body smear was fixed with Carnoy's fixative for 2 min, rinsed with absolute ethanol, and then air-dried and stained with 7% (wt/vol) Giemsa stain in 0.02 M phosphate buffer (pH 6.9) for 30 min. The stain was washed off, and the slide was air-dried before viewing by light microscopy. WEV-infected larvae were homogenized in 0.02 M phosphate buffer (pH 6.2), were filtered through three layers of muslin, and then were loaded onto a 45–65% (wt/wt) stepwise sucrose gradient and centrifuged at 75,000 × *g* for 1 h in a Beckman-Coulter SW32 rotor. Bands containing spheroids and spindles were harvested, washed, and resuspended in H_2O.

WEV spheroids were treated with an equal volume of 1 M NaOH for 5 min and then were neutralized with the same volume of 1 M HCl. Viral DNA was phenol/chloroform extracted, ethanol precipitated, and resuspended in H_2O. A PCR product representing amino acids 8–229 of the mature WEV fusolin sequence was obtained using degenerate primers to conserved regions of fusolin genes designated "fusup" (5′-TATAGCIAGRCAAAGAAGATGTTC-3′), and "fuslow" (5′-AACGCAATTATAAAATCCTTCWCC-3′). The coding sequence for amino acids 216–309 of fusolin was amplified using a specific primer, WEVFusintF (5′- GCAAAGAATAGATCCTGTAGG-3′), designed from the previously amplified N-terminal fragment, and WEVdgenR (5′-YTTRTTRTAGACRTACTGGTG-3′), a degenerate primer elucidated from a peptide sequence generated by MS analysis of purified WEV spindles that was identified by sequence comparison as being at or near the C terminus of fusolin. The PCR products were gel purified and then were cloned into the plasmid vector pGEMTeasy and sequenced. Clones were confirmed as WEV fusolin by sequence homology and MS analysis of purified fusolin.

WEV spindles were denatured and electrophoresed on a 10% SDS/PAGE gel, and the band corresponding to the fusolin protein was extracted and submitted to the Centre for Protein Research, University of Otago, for in-gel trypsin digestion and MS analysis on an LC-MALDI TOF/TOF mass spectrometer. Protein identification was performed using the Mascot search engine against the protein sequence deduced by translation of the DNA sequence. De novo sequencing also was performed using the chemically assisted fragmentation technique. Sequences were generated by MALDI-based tandem MS and were interpreted individually.

Alternatively the SDS/PAGE gels were transferred to Immobilon PVDF membrane (Millipore), stained with Coomassie G-250, then destained in 50% methanol and rinsed overnight in H_2O before excision of the fusolin band and N-terminal sequencing by Edman degradation. The N terminus was confirmed by 4-sulfophenyl isothiocyanate–labeled MS of solubilized fusolin.

Data Collection and Structure Determination. X-ray diffraction experiments were conducted at the MX2 beamline (Australian synchrotron) with a collimated beam of 20 × 20 μm, and at the X06SA microfocus beamline (Swiss Light Source) using the MD2 diffractometer with a collimated beam of 15 × 5 μm that was focused on the detector.

Data were collected at 100 K using spindles that were transferred into 50 mM MES (pH 6.0) and 50% ethylene glycol and subsequently were spread onto micromeshes (MiTeGen). Diffraction images were processed using HKL-2000 (HKL Research), and data from multiple isomorphous crystals were scaled using SCALEPACK (3). Subsequent data manipulation and model analyses were done primarily with the CCP4 suite (4).

The structure of MMEV fusolin was determined by molecular replacement using the CBP21 protein (PDB ID code: 2BEM). This model has only low sequence similarity (14% identity/27% similarity over 237 residues) and represented only ∼60% of MMEV fusolin. Although the orientation of the model was identified correctly by PHASER (5), the resulting electron density map did not allow rebuilding of the MMEV fusolin model. The Rosetta ab initio molecular replacement implementation in PHENIX (rosetta_mr) (6) was used to produce interpretable maps using 9- and 3-mer fragment libraries. These libraries were generated using the Robetta fragment server (robetta.bakerlab.org/fragmentsubmit.jsp) and an alignment file of the search models generated by the HHPRED server (toolkit.tuebingen.mpg.de/hhpred). The search models included the following structures: 2BEM, 3KM5, 2YTC, 1UOZ, 3EJA, 2OL3, 1PKO, 3BIK, 3O0L, and 1OC7.

The structures of the ACEV and WEV fusolins then were determined by molecular replacement using PHASER (5) with a poly-Ala version of PDB ID code 2BEM. The initial molecular replacement solution was improved by multiple cycles of density modification together with poly-Ala chain tracing using SHELXE (7). The poly-Ala model was extended and sequence assigned by ARP/wARP (8). WEV was determined by molecular replacement using an initial ACEV model. SHELXE was used for density modification and poly-Ala chain tracing. An initial model was built by the program ARP/wARP.

The models were rebuilt in COOT (9) and refined with BUSTER 2.10 (10). The first 18 residues correspond to the signal sequence and are proteolytically removed after translocation into the endoplasmic reticulum in all fusolins. Numbering starts from the first residue of the mature fusolin protein (His_1). The MMEV fusolin includes residues 1–260, 312–317, and 328–369. The main missing region is a region of low sequence complexity containing a large number of Tyr-Glu-Asn repeats and predicted to be disordered. The final MMEV model has very good crystallographic statistics and protein geometry that fall within the 99th percentile of the MolProbity score. All residues lie in the allowed regions of the Ramachandran plot.

Data collection and refinement statistics for the three fusolin models are presented in Table S1. Crystal contacts and oligomeric interfaces were analyzed using the PISA service (11) at the European Bioinformatics Institute (www.ebi.ac.uk/pdbe/prot_int/pistart.html).

Soaks of Spindles in Solutions of Zinc and Copper Ions. To determine the fusolin structure in presence of a metal, the spindles (1 μL in 30 μL and 50 μL of water for copper and 1 μL in 50 μL water for zinc) were soaked with 2 mM of $CuSO_4$ and $ZnSO_4$ (Sigma-Aldrich) for 24 h. Then 0.3 μL of the mix was mounted on micromeshes (MiTeGen), the excess was removed, and 0.3 μL of a 50% ethylene glycol cryo-solution was added on the micromesh. The excess liquid was removed, and the micromesh was flash-frozen in liquid nitrogen. The structures of copper- and zinc-soaked spindles were refined using the best datasets up to a resolution of 2.4 Å (Table S2).

To determine the nature of the metal bound to fusolin, datasets were collected below and above the expected K edges of copper and zinc. For these diffraction experiments, 1 μL of spindles was soaked in 30 μL of 2 mM $CuSO_4$ and incubated for 24 h. Similarly, 1 μL of spindles was soaked for 24 h in 100 μL of 2 mM $ZnSO_4$.

Diffraction data were collected as described above at resolution limits between 2.4 and 3.1 Å (see Fig. S4*C* for details). Anomalous maps at 8.500 keV (remote) and 8.991 keV (peak) for copper and 9.2 keV (remote) and 9.671 keV (peak) for zinc were generated using the FFT program of the CCP4 suite.

Spindle Dissolution Patterns. For analytical size-exclusion chromatography, 500 μg of MMEV spindles were washed in water, dissolved in 50 mM sodium carbonate (pH 13), and subjected to size-exclusion chromatography–multi-angle laser light scattering (SEC-MALLS) using a Superdex 200 10/300 column (GE Healthcare) equilibrated in 50 mM sodium carbonate (pH 10), 200 mM NaCl, and 25 mM β-mercaptoethanol. The chromatographic system consisted of a Shimadzu DGU-20A5 degasser, LC-20AD liquid chromatograph, SIL-20AHT auto-sampler, CBM-20A communications bus module, SPD-20A UV/VIS detector, and CTO-20AC column oven, coupled to a Wyatt Technology DAWN HELEO-II light-scattering detector fitted with an Optilab T-rEX refractive index detector. Calibration of the system was established using BSA (Sigma-Aldrich). Data collection and analysis were performed with the ASTRA software (Wyatt Technology).

For dissolution, 40 μg of spindles were washed in milliQ water and incubated in 4 μL NaOH (pH 13). The dissolved spindles were diluted in 36 μL sodium carbonate (pH 10) to allow proteolysis analysis. This solution was subjected to proteolysis for up to 2 h at 30 °C by the addition of 0.4 μg α-chymotrypsin (i.e., 1:100, wt/wt) Sigma-Aldrich) previously dissolved in water and 10 mM $CaCl_2$.

Detailed Structure Description. As anticipated from the high amino acid sequence similarities (~58% cross-sequence identities between MMEV, ACEV, and WEV fusolin), the three fusolin structures are very similar, with rmsds below 1 Å for all atoms from equivalent residues. Fusolin is organized in two domains, a compact N-terminal domain followed by a C-terminal V-shaped extension (Fig. 1*A*). A linker of variable length depending on the virus species connects the two domains. The N-terminal domain of fusolin adopts a modified Fn3 fold composed of an anti-parallel β-sandwich with ABE-GFCD topology (the strand labels are ordered according to the primary sequence). Two short strands, $\beta_{A'}$ and $\beta_{A''}$, extend the GFCD sheet, almost closing the sandwich into a β-barrel. Both these short strands pack against strand G but are arranged head-to-tail.

A helical subdomain of ~112 residues forms a wedge-shaped projection on one side of the β-sandwich. This projection subdomain is inserted in the AB loop in the Fn3 fold and is stabilized by two disulfide bonds formed between cysteines C_{14}–C_{34} and C_{93}–C_{228}. The β-sandwich contains an additional disulfide bond C_{139}–C_{189} maintaining loop DE (residues 177–195) in a flap over the small β-sheet (Fig. 1).

The linker that follows the N-terminal domain positions the four-turn helix H5 ~20 Å away from the core of the molecule in an orientation that is roughly orthogonal to the β-sandwich (Fig. 1*A*). This linker varies in length and sequence among fusolin proteins and has various degrees of disorder in our three structures (Fig. S1). WEV fusolin has the shortest linker, 35 residues (232–266). In this structure, the linker is clearly visible apart from a small section corresponding to residues 247–251, so that the connectivity between the two domains is unambiguous. In contrast, MMEV fusolin has a much larger linker consisting of 93 residues (235–328), including eight repeats characterized by a sequence motif YENN/D. The absence of interpretable electron density for these YEN repeats suggests that this region either is dynamic or adopts multiple conformations in spindles.

In spindles, two fusolin molecules form a stable dimer centered on a twofold crystallographic axis (Fig. 1*B*). A striking feature of this dimer is domain swapping of the amphipathic helix H5 that fits into a hydrophobic groove of the β-sandwich of a neighboring molecule. This groove extends from one side of the sandwich to the projection domain. In particular, strand $\beta_{A''}$ and the DE flap form a tight clamp around the C-terminal end of helix H5. The dimeric interface is relatively extended with a buried area of 3,530 $Å^2$, representing 36% of the accessible surface of the fusolin protein. Fifty-four hydrogen bonds and eight salt bridges contribute to the stability of the assembly. The CT extension is involved in a majority of these interactions, forming a large V-shaped footprint on the projection domain of the other subunit of the dimer (Fig. S7).

Comparison with Cellular Homologs. The closest structural homolog of fusolin is the bacterial protein CBP21 [PDB ID code: 2BEM (12)]. The topology and fold of fusolin closely match that of CBP21 with an rmsd of 1.55 Å over 145 equivalent residues [Secondary Structure Matching (SSM) Z-score = 9.4]. This similarity is particularly strong for the core of the β-sandwich of the Fn3 domain. When present, C-terminal extensions to AA10 proteins bear no similarity to the CT extension, which has no structural homolog in the PDB. The projection region within the Fn3 domain is larger in fusolin than in CBP21 (~112 residues vs. 60 residues) because of an inserted helix-turn-helix motif just after disulfide bond C_{14}–C_{34} that also stabilizes the projection domain of CBP21 (Fig. 2).

A buried salt bridge between R_{10} and D_{230} stabilizes the packing of the projection domain onto the side of the β-sandwich for all AA10 proteins. Residue Arg_{10} also forms a pi interaction with Trp_{117}, another strictly conserved residue in AA10 proteins. In more distantly related AA9 proteins such as Cel61B of the filamentous fungus *Hypocrea jecorina* (13) (PDB ID code: 2VTC), the absence of this salt bridge is compensated by a disulfide bond between the two subdomains. Interestingly, this disulfide bond is equivalent to the disulfide bond C_{93}–C_{228} in fusolin that is stabilized by both of these bridging interactions.

LPMO Active Site. In WEV spindles electron density corresponding to an undetermined metal is present and was modeled as Zn^{2+}. In the two other structures the corresponding site was unoccupied but could be populated by incubation of MMEV spindles in either $CuSO_4$ or $ZnSO_4$ without significant conformational changes upon binding (Fig. S5). The coordination observed in fusolin is similar to other AA10 proteins of *Enterococcus faecalis* V583 (PDB ID code: 4ALT) (14) and *Bacillus amyloliquefaciens* (PDB ID code: 2YOX) (15) with an rmsd of 0.3 Å and 0.5 Å, respectively, for conserved residues within 6 Å of the metal (Fig. S5).

A rim of polar and acidic residues around the metal site is equivalent to residues in CBP21 that participate to substrate binding as shown by site-directed mutagenesis (e.g., Glu_{33}/Asp_{155}/Asn_{158} vs. Asp_{219}/Glu_{223} in fusolin) (16) or deuterium exchange (e.g., Glu_{28}/Gln_{30}/Ser_{31}/Thr_{84} vs. Gln_{65}/Asn_{67}/Glu_{68}/Thr_{141} in fusolin) (Fig. 2 and Fig. S3*A*) (17). The rims are structurally and chemically similar around His_1 and Thr_{141}—which are strictly conserved in all AA10 proteins—but the opposite side differs in its conformation, in part because of the presence of arginine Arg_{217} in fusolin instead of a buried isoleucine in CBP21. However, compensating rearrangements mean that the carboxylate moieties of Asp_{219} and Glu_{223} of fusolin adopt equivalent conformations to Asp_{155} and Glu_{33} of CBP21 at 8–9 Å and 6 Å, respectively, from His_{144}.

Directly adjacent to the polar rim, the fusolin projection domain forms a flat platform complementary to crystalline chitin with two prominent tryptophans, Trp_{21} and Trp_{22} (Fig. 2 and Fig. S6). This surface-exposed di-tryptophan motif is structurally equivalent to Tyr_{54} of CBP21, which is involved in chitin binding as shown both by site-directed mutagenesis (16) and deuterium exchange (17). This motif also is reminiscent of the di-tyrosine motif that directly participates in polysaccharide binding in fungal LPMO-1 proteins (e.g., PDB ID code 3EII) (18).

Assembly of Spindles. In spindles, all fusolin molecules are identical, because their organization conforms to $P4_12_12$ crystallographic symmetry with one molecule in the asymmetric unit. The apparent cavities in the crystal structure are occupied by disordered loops in MMEV fusolin and glycans in the ACEV and WEV fusolins. The resulting crystalline matrix is relatively dense, with 33–38% solvent content if only the protein content is taken into account.

The supramolecular organization of spindles is based on the interactions of interconnected dimeric building blocks. A central dimer is surrounded by two structures: two crowns of four dimers encasing the dimer and two capping dimers, each at the center of a crown (Fig. 3). The crown dimers have only weak intermolecular interactions, and this structure is not predicted to be stable in solution by PISA analysis. In contrast, the two crowns are tightly connected to each other through the CT extensions. Two small segments comprising residues 313–316 and 364–369 connect the two crowns, and both are covalently crosslinked by stabilizing interdimer disulfide bonds.

The capping dimers are located on the outer sides of the crowns along a 2(1) axis passing through the center of the unit cell (Fig. 3). They reach through the middle of the crowns to establish covalent interactions with the central dimer. Because there is only one fusolin molecule in the asymmetric unit of the crystal, these interactions are, in fact, the same interactions that connect the two crowns and rely exclusively on the CT extension.

The interdimer interfaces stabilizing spindles are relatively large and overlap with both subunits. In MMEV spindles disulfide bonds between dimers form a 3D network that covalently crosslinks the entire crystal into a single polymer. Although there are no intradimer disulfide bonds, each subunit is covalently linked to four other molecules so that overall every dimer is disulfide bonded to six adjacent dimers (Fig. 3*C*). This network also may be present in ACEV, although disulfide bounds are not visualized in our structure because of missing electron density. The cysteines involved in interdimer crosslinking in MMEV and ACEV spindles are not conserved in WEV spindles, but an alternate interdimer disulfide bond exists between Cys_{80} and Cys_{255}.

Essential Structural Role of the CT Extension in Spindles. Within the CT extension, helix H5 is primarily involved in the dimeric interface rather than interdimer interactions. In contrast, the regions flanking helix H5 mediate multiple interactions between fusolin dimers. In particular, the small section comprising residues 355–368 interacts with three other molecules in the crystal. Although two of these molecules have only small interaction surfaces, both contacts involve intermolecular disulfide bonds (Cys_{366}–Cys_{252} and Cys_{360}–Cys_{259}; Cys_{367}–Cys_{316}). Similarly, the linker region between the Fn3 domain and H5 (residues 241–260 and 312–316) interacts with five different molecules, forming intermolecular disulfide bonds with two of them (Cys_{252}–Cys_{366} and Cys_{259}–Cys_{360}; Cys_{316}–Cys_{367}).

Given the apparent central role of the CT extension in the crystalline organization, we analyzed the predicted stability of spindles when this region is omitted from the model (Fig. 7 *B*, *D*, and *F*). Such a truncated fusolin would have interface areas with neighboring molecules of only 530 $Å^2$, 400 $Å^2$, and 380 $Å^2$ involving no disulfide bonds and 8, 0, and 5 hydrogen bonds, respectively. These interaction surfaces are typical of the nonbiologically relevant crystal contacts found in in vitro crystals produced for structural analysis, and no higher assemblies of this truncated fusolin would be predicted (Fig. 5*C* and Fig. S7).

1. Gauthier L, Cousserans F, Veyrunes JC, Bergoin M (1995) The Melolontha melolontha entomopoxvirus (MmEPV) fusolin is related to the fusolins of lepidopteran EPVs and to the 37K baculovirus glycoprotein. *Virology* 208(2):427–436.
2. Mitsuhashi W, Miyamoto K (2003) Disintegration of the peritrophic membrane of silkworm larvae due to spindles of an entomopoxvirus. *J Invertebr Pathol* 82(1):34–40.
3. Minor W, Cymborowski M, Otwinowski Z, Chruszcz M (2006) HKL-3000: The integration of data reduction and structure solution—from diffraction images to an initial model in minutes. *Acta Crystallogr D Biol Crystallogr* 62(Pt 8):859–866.
4. Winn MD, et al. (2011) Overview of the CCP4 suite and current developments. *Acta Crystallogr D Biol Crystallogr* 67(Pt 4):235–242.
5. McCoy AJ, et al. (2007) Phaser crystallographic software. *J Appl Cryst* 40(Pt 4):658–674.
6. Terwilliger TC, et al. (2012) phenix.mr_rosetta: Molecular replacement and model rebuilding with Phenix and Rosetta. *J Struct Funct Genomics* 13(2):81–90.
7. Sheldrick GM (2008) A short history of SHELX. *Acta Crystallogr A* 64(Pt 1):112–122.
8. Langer G, Cohen SX, Lamzin VS, Perrakis A (2008) Automated macromolecular model building for X-ray crystallography using ARP/wARP version 7. *Nat Protoc* 3(7):1171–1179.
9. Emsley P, Lohkamp B, Scott WG, Cowtan K (2010) Features and development of Coot. *Acta Crystallogr D Biol Crystallogr* 66(Pt 4):486–501.
10. Blanc E, et al. (2004) Refinement of severely incomplete structures with maximum likelihood in BUSTER-TNT. *Acta Crystallogr D Biol Crystallogr* 60(Pt 12 Pt 1):2210–2221.
11. Krissinel E, Henrick K (2007) Inference of macromolecular assemblies from crystalline state. *J Mol Biol* 372(3):774–797.
12. Vaaje-Kolstad G, Houston DR, Riemen AHK, Eijsink VGH, van Aalten DMF (2005) Crystal structure and binding properties of the Serratia marcescens chitin-binding protein CBP21. *J Biol Chem* 280(12):11313–11319.
13. Karkehabadi S, et al. (2008) The first structure of a glycoside hydrolase family 61 member, Cel61B from Hypocrea jecorina, at 1.6 A resolution. *J Mol Biol* 383(1): 144–154.
14. Gudmundsson M, et al. (2014) Structural and electronic snapshots during the transition from a Cu(II) to Cu(I) metal center of a lytic polysaccharide monooxygenase by X-ray photoreduction. *J Biol Chem* 289(27):18782–18792.
15. Hemsworth GR, et al. (2013) The copper active site of CBM33 polysaccharide oxygenases. *J Am Chem Soc* 135(16):6069–6077.
16. Vaaje-Kolstad G, Horn SJ, van Aalten DMF, Synstad B, Eijsink VGH (2005) The non-catalytic chitin-binding protein CBP21 from Serratia marcescens is essential for chitin degradation. *J Biol Chem* 280(31):28492–28497.
17. Aachmann FL, Sørlie M, Skjåk-Bræk G, Eijsink VGH, Vaaje-Kolstad G (2012) NMR structure of a lytic polysaccharide monooxygenase provides insight into copper binding, protein dynamics, and substrate interactions. *Proc Natl Acad Sci USA* 109(46): 18779–18784.
18. Harris PV, et al. (2010) Stimulation of lignocellulosic biomass hydrolysis by proteins of glycoside hydrolase family 61: Structure and function of a large, enigmatic family. *Biochemistry* 49(15):3305–3316.

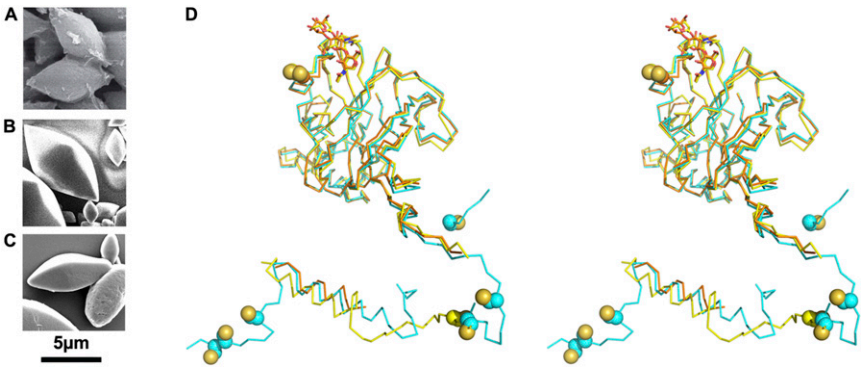

Fig. S1. Comparison of the three fusolin structures. (*A*–*C*) Scanning EM pictures of MMEV, ACEV, and WEV spindles. (*D*) Wall-eye stereo representation of the fusolin proteins. The ribbon diagrams of fusolins produced by MMEV, ACEV, and WEV are colored in cyan, orange, and yellow respectively. Cysteines involved in intermolecular disulfide bonds are shown as spheres, and glycosylations in ACEV and WEV fusolins are shown as sticks. Cysteines involved in the disulfide network in MMEV are also present in ACEV, although the disulfide bounds are not visualized in our structure because of missing electron density. They are not present in WEV spindles, but an alternate interdimer disulfide bond between Cys_{80} and Cys_{255} plays a similar role.

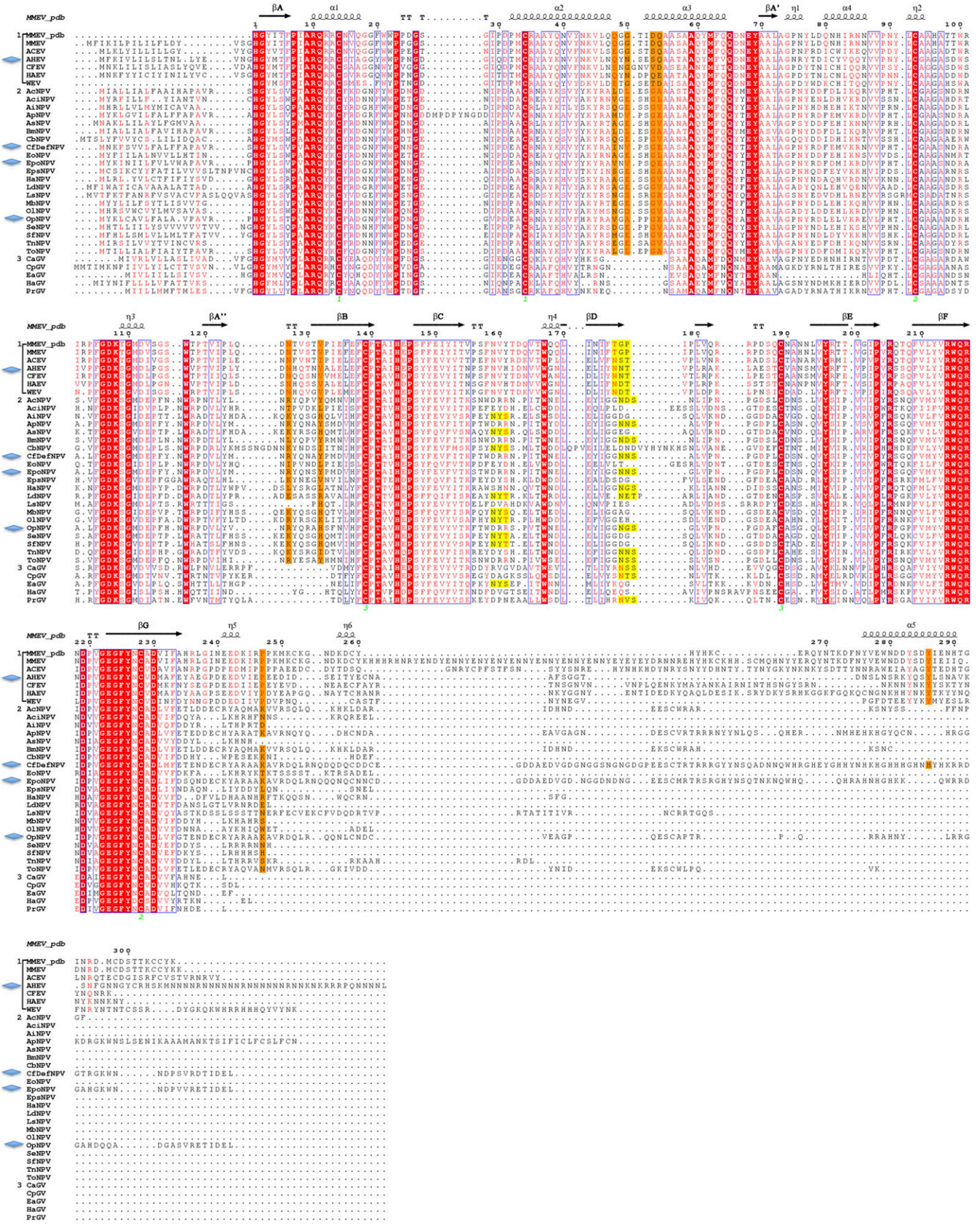

Fig. S2. Multiple sequence alignment of viral AA10 proteins. A nonredundant sequence alignment of 32 sequences of fusolin and fusolin-like proteins was constructed using ClustalW and processed with ESPript as three groups representing EV, α-, and β-baculoviruses. Numbering and secondary structures

Legend continued on following page

correspond to the MMEV fusolin. Secondary structure elements calculated by the DSSP program are labeled above the alignment. Residues in white characters on a red background are strictly conserved; residues in black bold characters are similar within a group; residues in blue frames are similar across groups; and residues on an orange background are dissimilar among conserved groups. Cysteine residues involved in intramolecular disulfide bonds are indicated with matching numbers 1–3 in green under the sequences. Glycosylation sites are highlighted in yellow. Viruses that produce spindle-like crystals are indicated in the alignment by a diamond before the abbreviated name: *Choristoneura fumiferana* DEF nuclear polyhedrosis virus (NPV) (1) [82% identical to *Choristoneura murinana* NPV (2); not shown], *Epiphyas postvittana* NPV (3), and *Orgyia pseudotsugata* NPV (4). Group 1, EV: MMEV, *Melolontha melolontha* EV [GenBank Identifier (GI): 987084]; ACEV, *Anomala cuprea* EV (GI: 3059217); AHEV, *Adoxophyes honmai* EV (GI: 506498228); CFEV, *Choristoneura fumiferana* EV (GI: 4098252); HAEV, *Heliothis armigera* EV (GI: 329566); WEV, *Wiseana spp* EV (PDB ID code: 4YN2). Group 2, α-baculovirus: AcNPV, *Autographa californica* NPV (GI: 9627807); AciNPV, *Apocheima cinerarium* NPV (GI: 402502149); AiNPV, *Agrotis ipsilon* NPV (GI: 09170914); ApNPV, *Antheraea pernyi* NPV (GI: 96979851); AsNPV, *Agrotis segetum* NPV (GI: 90592743); BmNPV, *Bombyx mori* NPV (GI: 9630871); CbNPV, *Clanis bilineata* NPV (GI: 113195457); CfDefNPV, *Choristoneura fumiferana DEF* NPV (GI: 37651359); EoNPV, *Ectropis obliqua* NPV (GI: 118197530); EpoNPV, *Epiphyas postvittana* NPV (GI: 15320714); EpsNPV, *Euproctis pseudoconspersa* NPV (GI: 228861610); HaNPV, *Helicoverpa armigera* NPV (GI: 209401112); LdNPV, *Lymantria dispar* NPV (GI: 9631035); LsNPV, *Leucania separata* NPV (GI: 2760659); MbNPV, *Mamestra brassicae* NPV (GI:5565847); OlNPV, *Orgyia leucostigma* NPV (GI:165969039); OpNPV, *Orgyia pseudotsugata* NPV (GI: 9630007); SeNPV, *Spodoptera exigua* NPV (GI: 9634246); SfNPV, *Spodoptera frugiperda* NPV (GI: 319997357); TnNPV, *Trichoplusia ni* NPV (GI: 74229750); ToNPV, *Thysanoplusia orichalcea* NPV (GI: 438000366). Group 3, β-baculovirus: CaGV, *Clostera anachoreta* GV (GI: 334265691); CpGV, *Cydia pomonella* GV (GI: 14602254); EaGV, *Epinotia aporema* GV (GI: 410493600); HaGV, *Helicoverpa armigera* GV (GI: 164519304); PrGV, *Pieris rapae* GV (GI: 288804652).

1. Li X, et al. (2000) Characterization of an overexpressed spindle protein during a baculovirus infection. *Virology* 268(1):56–67.
2. Huger AM, Krieg A (1968) On spindle-shaped cytoplasmic inclusions associated with a nuclear polyhedrosis of Choristoneura murinana. *J Invertebr Pathol* 68(5):1251–1260.
3. MacCollom GB, Reed EM (1971) A nuclear polyhedrosis virus of the light brown apple moth, Epiphyas postvittana. *J Invertebr Pathol* 18(3):337–343.
4. Gross CH, Wolgamot GM, Russell RL, Pearson MN, Rohrmann GF (1993) A 37-kilodalton glycoprotein from a baculovirus of Orgyia pseudotsugata is localized to cytoplasmic inclusion bodies. *J Virol* 67(1):469–475.

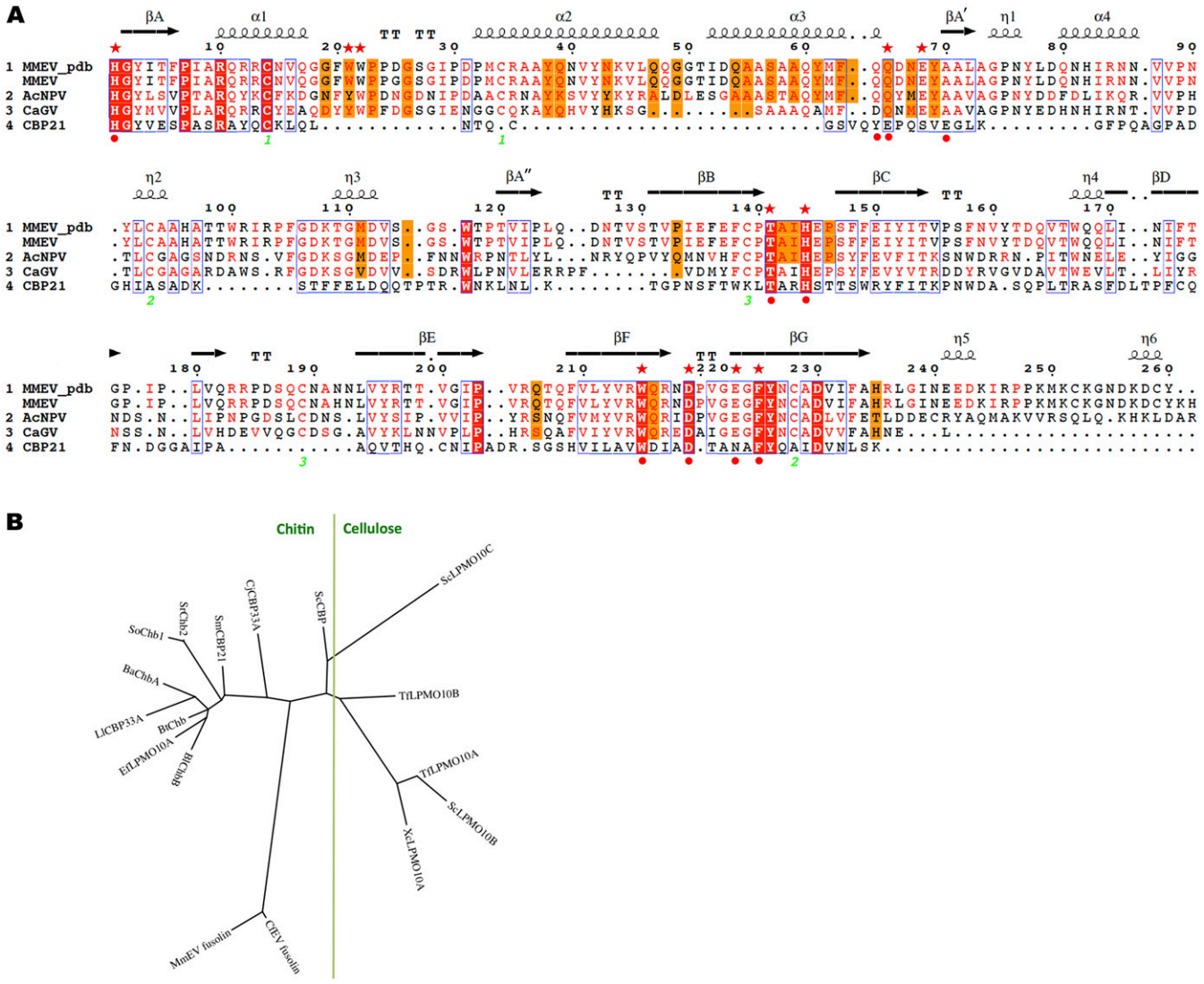

Fig. S3. Fusolin has the hallmarks of a lytic chitin monooxygenase. (*A*) Sequence alignment of the Fn3 domains of fusolin homologs. Sequences were aligned with ClustalW for viral proteins (see Fig. S2 for a full alignment) and with PDBFold for CBP21. In the ESPript alignment only one representative sequence for each group is shown corresponding to EV fusolins (MMEV), α-baculoviruses GP37 (AcNPV), β-baculoviruses GP37 (CaGV), and CBP21. Residues in white characters on a red background are strictly conserved; residues in bold characters are similar within a group; residues in blue frames are similar across groups; and residues on an orange background are dissimilar among conserved groups [EV, NPV, granulosis virus (GV), and CBP21]. Secondary structure elements calculated by the DSSP program for MMEV fusolin are represented above the alignment. Red stars and circles denote residues shown in Fig. 2 *C* and *F*, respectively. (*B*) Phylogeny of a Coleopteran EV fusolin (MmEV) and a Lepidopteran EV fusolin (CfEV) compared with 14 AA10 lytic polysaccharide monooxygenases that have been functionally characterized (1). Phylogenetic analysis was carried out using Phylogeny.fr. The proteins are divided in two groups related to their substrate affinity The chitin-binding protein group comprises BaChbA [*Bacillus amyloliquefaciens*, UniProt (UNP) ID: Q9F9Q5], SrChb2 (*Streptomyces reticuli*, UNP ID: O87962), SoChb1 (*Streptomyces olivaceoviridis*, UNP ID: Q54501), BlChbB (*Bacillus licheniformis*, UNP ID: Q62YN7), SmCBP21 (*Serratia marcescens*, UNP ID: O83009), ScCBP (*Streptomyces coelicolor*, GI: 499338237), MmEV_fusolin (*Melolontha melolontha* EV, GI: 987084), CfEV_fusolin (*Choristoneura fumiferana* EV, GI: 4098252), BtChb (*Bacillus thuringiensis* subsp. *konkukian*, UNP ID: Q6HHR5), CjCBP33A (*Cellvibrio japonicus*, UNP ID: B3PJ79), EfLPMO10A (*Enterococcus faecalis* CBM33, UNP ID: Q838S1), and LlCBP33A (*Lactococcus lactis* subsp. *Lactis,* GI: 15673933). The cellulose-binding protein group comprised ScLPMO10B (*Streptomyces coelicolor*, UNP ID: Q9RJC1), ScLPMO10C (*Streptomyces coelicolor* CelS2, UNP ID: Q9RJY2), TfLPMO10A (*Thermobifida fusca,* UNP ID: Q47QG3), TfLPMO10B (*Thermobifida fusca,* UNP ID: Q47PB9), and XcLPMO10A (*Xylanimonas cellulosilytica*, GI: 502642591).

1. Forsberg Z, et al. (2014) Structural and functional characterization of a conserved pair of bacterial cellulose-oxidizing lytic polysaccharide monooxygenases. *Proc Natl Acad Sci USA* 111(23):8446–8451.

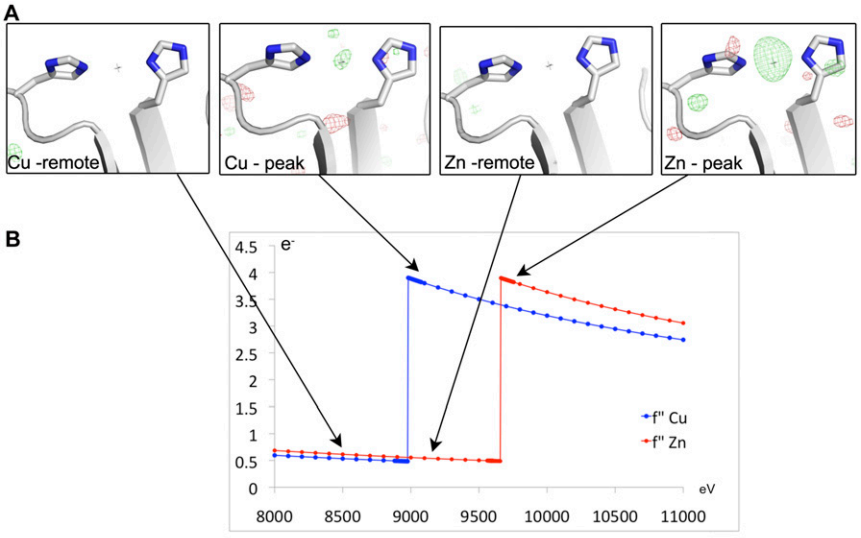

	Cu - remote	Cu - peak	Zn - remote	Zn - peak
Soak	2mM $CuSO_4$		2mM $ZnSO_4$	
Energy (eV)	8500	8991	9200	9671
f''_{Cu} (theoretical)	0.5	3.9	3.7	3.4
f''_{Zn} (theoretical)	0.6	0.5	0.5	3.9
Anomalous peak (σ)	✗ (<1.3)	✓(3.2)	✗ (<0.1)	✓ (7.5)
Resolution (Å)	28.6-2.8	27.2-2.4	29.6-3.1	27.3-2.4
Redundancy	7.4	7.2	3.6	3.1
Completeness (%)	99.8	98.0	90.3	96.2
I/σ	11.6	6.4	5.8	6.2

Fig. S4. MMEV spindles bind copper and zinc. (*A*) View of the metal-binding site with side chains of residues coordinating the metal represented as sticks. A gray cross represents the metal. The electron density of anomalous maps is shown at thresholds of −3σ (red) and +3σ (green). (*B*) Plot of the theoretical f′′ values for copper and zinc at energies between 8 and 11 keV. (*C*) Table summarizing statistics for each dataset and anomalous maps.

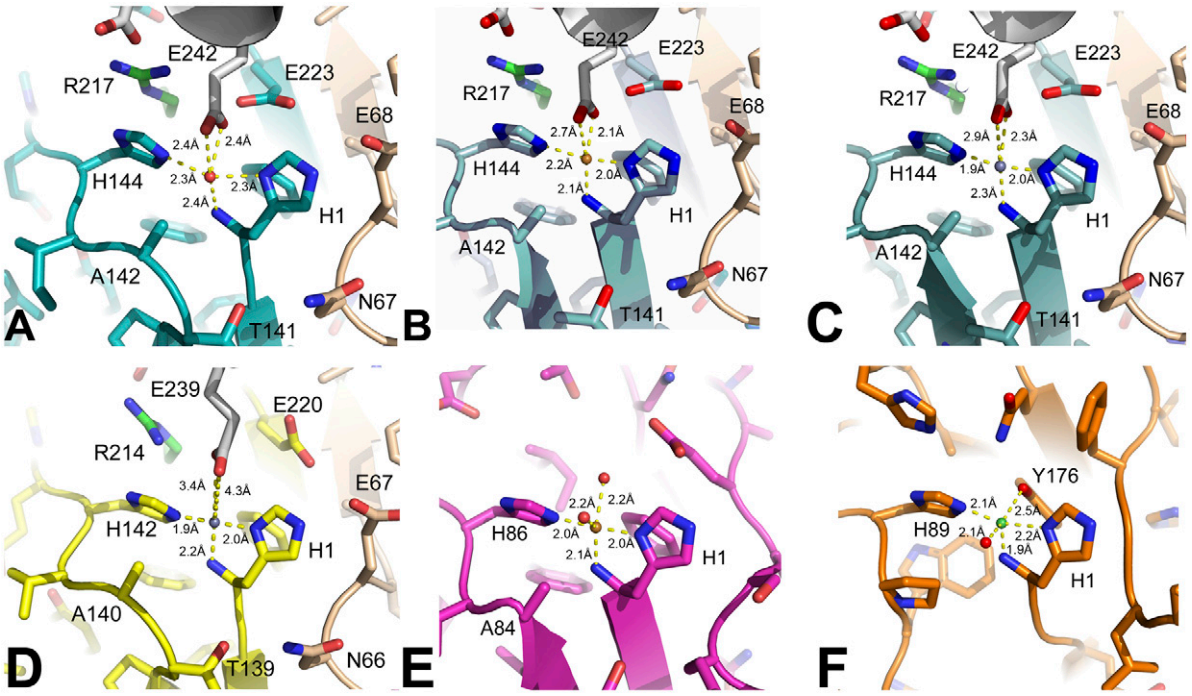

Fig. S5. The metal-binding site of fusolin. The metal-binding site is shown with side chains of residues coordinating the metal represented as sticks. Non-protein atoms coordinated by the two conserved histidines are represented as spheres colored in red for water molecules, brown for copper, gray for zinc, and green for nickel. The first row (*A*–*C*) represents the MMEV fusolin directly purified from infected insects (*A*), after a 24-h soak in 2 mM $CuSO_4$ (*B*), or after a 24-h soak in 2 mM $ZnSO_4$ (*C*). (*D*) The WEV fusolin directly purified from infected insects with an unidentified metal modeled as a zinc ion. (*E* and *F*) For comparison, the next two panels represent another AA10 protein in complex with Cu^{2+}, EfaCBM33A of *Enterococcus faecalis* (PDB ID code: 4ALC) (*E*), and an AA9 protein in complex with Ni^{2+}, Cel61A from *Hypocrea jecorina* (PDB ID code: 2VTC) (*F*).

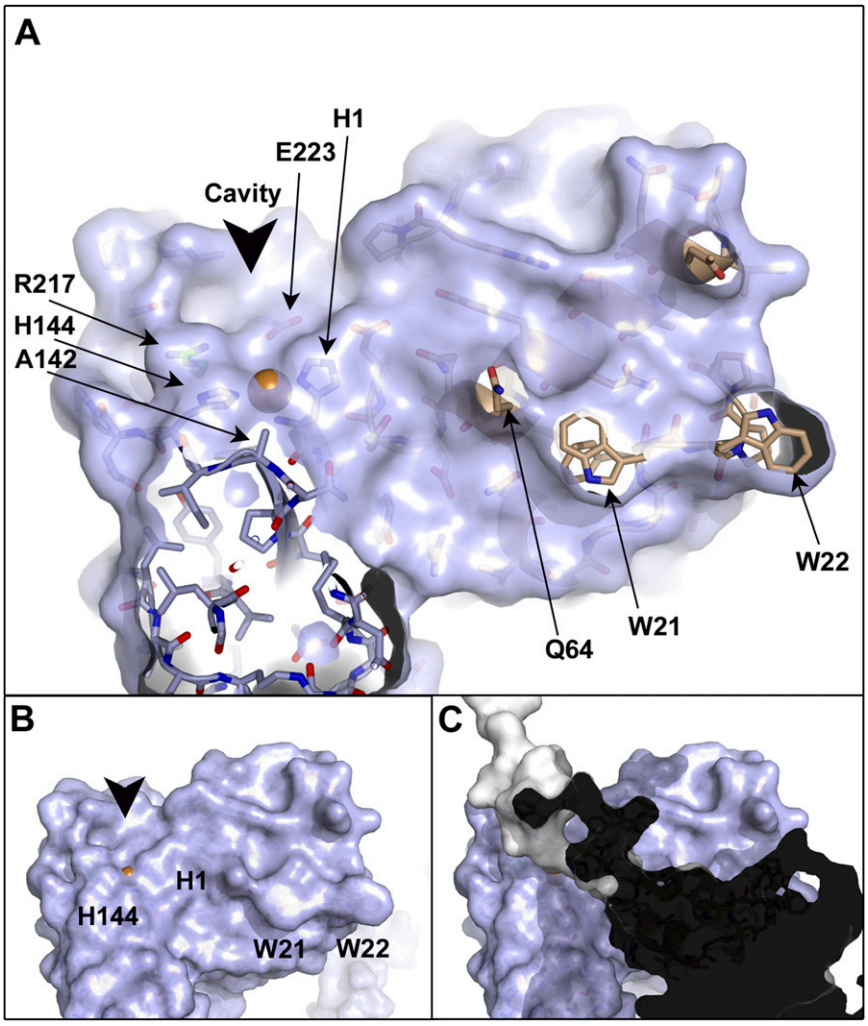

Fig. S6. The copper-binding site of fusolin is occluded in the assembled spindle. (*A*) Surface representation of fusolin. The Cu^{2+} ion is shown as a brown sphere. The shallow depth of view highlights a cavity next to the Cu^{2+} ion and the flat platform including the di-tryptophan motif that may participate to substrate binding. (*B*) The view shown in *A* with a greater depth of view. (*C*) The view shown in *B* including the symmetry-related molecule colored in white that occludes the putative active site in assembled spindles.

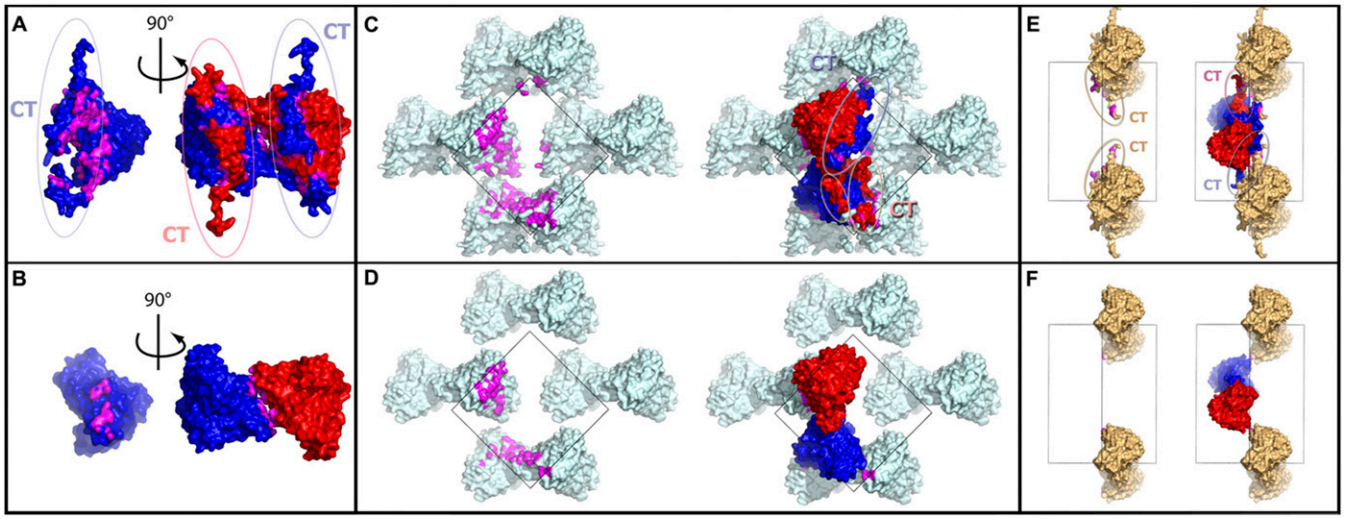

Fig. S7. The CT extension mediates spindle assembly. Crystal contacts shown in magenta are compared in the full-length fusolin (*A*, *C*, and *E*) and a protein lacking the CT extension (*B*, *D*, and *F*). Without the CT extension, fusolin is not predicted to dimerize (*A* and *B*), and the surface areas involved in crystal contacts with the crown dimers (*C* and *D*) and capping dimers (*E* and *F*) are minimal.

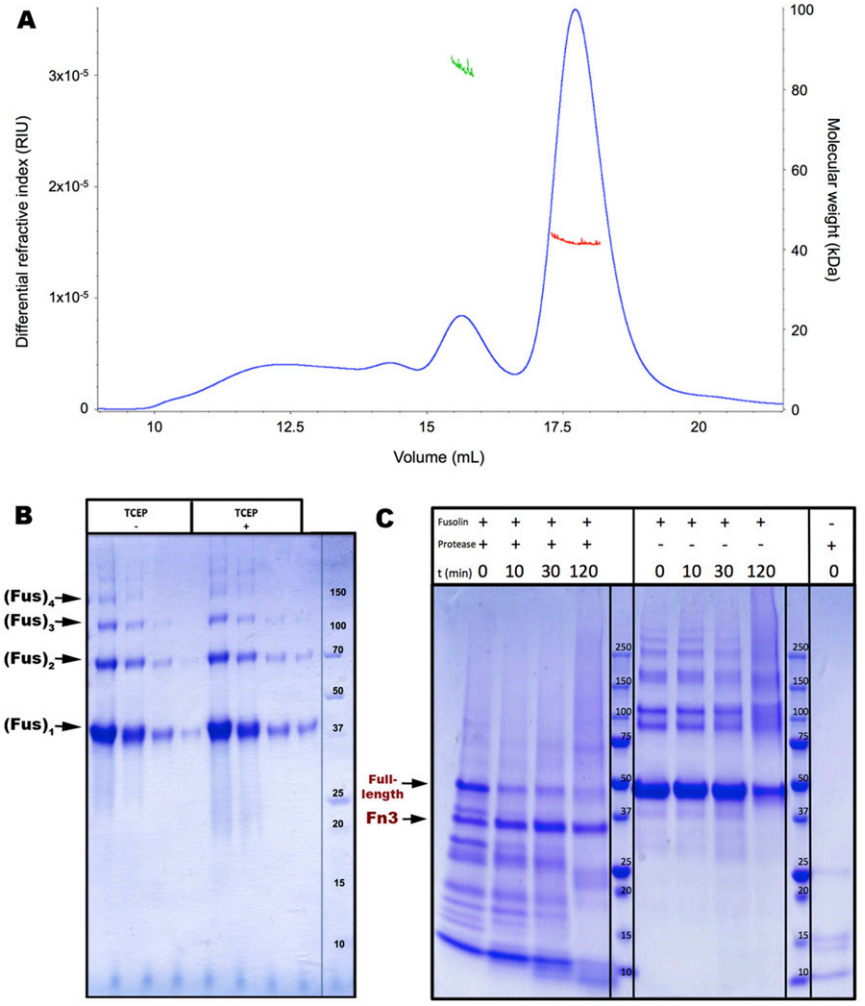

Fig. S8. SDS PAGE-resistant oligomers of fusolin dissociate upon cleavage of the CT molecular arm by chymotrypsin. (*A*) S200 size-exclusion chromatography profile of dissolved spindles. Spindles were dissolved at pH 13 and loaded onto the S200 at pH 10. MALLS scattering data collected simultaneously with peak elution are shown above the protein trace. The deduced molecular masses of the two main species correspond to a monomer (41.8 kDa ± 1.7%, ~60% of total mass) and a dimer (85.4 kDa ± 3.1%, ~14% of total mass) of the fusolin protein. (*B*) Analysis by reducing SDS PAGE of 50, 25, 12.5, and 6.25 μg of MMEV spindles dissolved in 50 mM sodium carbonate (pH 13) in the absence or presence of 25 mM Tris(2-carboxyethyl)phosphine (TCEP). The lower band corresponds to the monomer $(Fus)_1$, and a ladder corresponding to higher oligomeric states can be observed. (*C*) Reducing SDS PAGE of MMEV spindles dissolved in NaOH pH13 and diluted 10 times in 100 mM sodium carbonate (pH 10) in the presence or absence of alpha chymotrypsin (1:100, wt/wt). All samples were incubated at 30 °C and were collected at time points 0, 10, 30, and 120 min. The full-length fusolin is digested progressively to a stable core with an estimated size corresponding to the Fn3 domain. Even at the earliest time point, SDS-resistant species are lost when incubated with chymotrypsin.

Table S1. Data collection and structure refinement statistics of native spindles

Statistics	MMEV	ACEV	WEV
Data collection			
Space group	$P4_12_12$	$P4_12_12$	$P4_12_12$
Wavelength, Å	1.0	1.0	1.0
Unit cell parameters, Å	a = b = 71.27, c = 129.57	a = b = 71.89, c = 128.0	a = b = 68.18, c = 128.1
Resolution range, Å	30–1.90 (1.97–1.90)	20–1.90 (1.97–1.90)	20–2.00 (2.13–2.00)
R_{sym}, %	26.5 (86.3)	19.2 (69.9)	18.3 (53.7)
<I/σ(I)>	10.6 (1.9)	12.7 (4.0)	8.7 (3.8)
Completeness, %	99.8 (98.7)	99.7 (100.0)	99.0 (95.8)
Multiplicity	13.9 (6.5)	17.5 (10.2)	8.3 (7.9)
Refinement			
Resolution range, Å	28.6–1.90 (1.98–1.90)	20–1.90 (1.98–1.90)	14.4–2.02 (2.13–2.02)
No. of reflections	26,786 (2,504)	27,386 (2,844)	20,125 (2,700)
R/R_{free}	16.8/20.3 (22.5/27.0)	16.8/19.9 (18.0/18.2)	16.8/19.9 (16.4/19.8)
No. of atoms (protein/solvent/ ethylene glycol/metal)	5,025 (4751/194/80/0)	4,402 (4133/ 239/30/ 0)	4,596 (4405/170/20/1)
Geometry statistics			
Rmsd bonds, Å	0.010	0.010	0.007
Rmsd angles, °	1.010	1.040	0.870
Average B-factor, $Å^2$ (protein/solvent/ ethylene glycol/metal)	22.96 (22.0/36.5/39.6/-)	20.9 (19.7/39.4/37.3/-)	18.8 (18.2/34.2/27.0/21.1)
Ramachandran plot (MolProbity)			
Favored, %	98.3	98.8	97.8
Allowed, %	1.7	0.8	2.2
Outliers, %	0	0.4	0

Numbers in parentheses correspond to the last resolution shell unless stated otherwise.

Table S2. Data collection and structure refinement statistics of spindles soaked with copper or zinc

Statistics	Cu-MMEV	Zn-MMEV
Data collection		
Space group	$P4_12_12$	$P4_12_12$
Wavelength, Å	1.378	1.278
Unit cell, Å	a = b = 71.49 c = 129.42	a = b = 71.79 c = 129.59
Resolution range, Å	27.25–2.4 (2.49–2.40)	27.31–2.4 (2.49–2.40)
Rsym, %	10.2 (35.6)	11.9 (37.7)
<I/sigma(I)>	6.37 (2.55)	6.21 (2.32)
Completeness, %	98.01 (92.61)	96.23 (89.19)
Multiplicity	2.0 (1.9)	1.8 (1.8)
Refinement		
No. of reflections	26,597 (2501)	24,688 (2355)
R/R_{free}	15.3/23.6 (20.1/29.2)	15.3/ 22.8 (19.3/ 29.0)
No. of nonhydrogen atoms (protein, metal, solvent)	2,709 (2,470/2/237)	2,643 (2,460/2/181)
Protein residues	307	306
Average B-factor, Å	16.2	16.0
Rms deviation bonds, Å	0.014	0.015
Rms deviation angles, °	1.72	1.74
Ramachandran plot (MolProbity)		
Favored, %	96.66	96.32
Allowed, %	3.34	3.68
Outliers, %	0	0

Numbers in parentheses correspond to the last resolution shell unless stated otherwise.